

Article

Antimicrobial Properties of Samarium Doped Hydroxyapatite Suspensions and Coatings

Simona Liliana Iconaru ^{1,*}, Andreea Groza ², Sofia Gaiaschi ³, Krzysztof Rokosz ⁴ , Steinar Raaen ⁵, Steluta Carmen Ciobanu ¹, Patrick Chapon ³ and Daniela Predoi ^{1,*}

¹ National Institute of Materials Physics, Atomistilor Street, No. 405A, P.O. Box MG 07, 077125 Magurele, Romania; ciobanucs@gmail.com

² National Institute for Laser, Plasma and Radiation Physics, 409 Atomistilor Street, P.O. Box MG 36, 077125 Magurele, Romania; andreeagroza75@gmail.com

³ HORIBA Jobin Yvon S.A.S., 6-18, Rue du Canal, 91165 Longjumeau, France; sofia.gaiaschi@horiba.com (S.G.); patrick.chapon@horiba.com (P.C.)

⁴ Division of Surface Electrochemistry & Technology, Faculty of Mechanical Engineering, Koszalin University of Technology, Raclawicka 15-17, PL 75-620 Koszalin, Poland; krzysztof.rokocz@tu.koszalin.pl

⁵ Department of Physics, Norwegian University of Science and Technology (NTNU), Realfagbygget E3-124 Høgskoleringen 5, NO 7491 Trondheim, Norway; steinar.raaen@ntnu.no

* Correspondence: simonaiconaru@gmail.com (S.L.I.); dpredoi@gmail.com (D.P.)

Received: 25 October 2020; Accepted: 17 November 2020; Published: 20 November 2020



Abstract: Post-implant infections are a major health problem, and it is well-known that treating them with conventional drugs is accompanied by many disadvantages. The development of new biomaterials with enhanced antimicrobial properties are of major interest for the scientific world. The aim of this study was to synthesize and characterize hydroxyapatite doped with Samarium ($\text{Ca}_{10-x}\text{Sm}_x(\text{PO}_4)_6(\text{OH})_2$, $x_{\text{Sm}} = 0.05$, 5Sm-HAp) suspensions, pellets and coatings. The 5Sm-HAp coatings on Si substrates were obtained by rf magnetron sputtering technique. The different techniques such as ultrasound measurements, scanning electron microscopy (SEM), Fourier transform infrared spectroscopy (FTIR), Glow Discharge Optical Emission Spectroscopy (GDOES), X-ray photoelectron spectroscopy (XPS) and atomic force microscopy (AFM) were used to examine the obtained coatings. The results showed that the doped Sm ions entered the structure of hydroxyapatite successfully and Sm ions was uniformly doped onto the surface of the support. The depth profile curves of Ca, P, O, H, Ce and Si elements exhibit their presence from a surface to substrate interface as function of sputtering time. XPS analysis indicated as calcium-phosphate structures enriched in Sm^{3+} ions. Furthermore, the antimicrobial properties of the 5Sm-HAp suspensions, targets and coatings were assessed against *Escherichia coli* ATCC 25922, *Staphylococcus aureus* ATCC 25923 and *Candida albicans* ATCC 10231. The results of the antimicrobial assays highlighted that that the samples presented a strong antimicrobial activity against the tested microbial strains. The results showed that the coatings after 48 h of incubation inhibited the growth of all tested microbial strains under the value of 0.6 Log CFU/mL. This study shows that the 5Sm-HAp samples are good candidates for the development of new antimicrobial agents.

Keywords: samarium doped hydroxyapatite; magnetron sputtering technique; antimicrobial activity

1. Introduction

Infections that can occur after implant surgery (dental implants or prostheses) are an important health problem. To solve this problem, researchers are making important efforts to find new biomaterials,

with improved physico-chemical and antimicrobial properties, that can be used in the biomedical field [1–7]. It is well-known that bone tissue consists of a minor organic part (30%) consisting mainly of collagen type I and a major inorganic part (~70%), consisting mainly in hydroxyapatite ($\text{Ca}_{10}(\text{PO}_4)_6(\text{OH})_2$, HAp). For the most common form of hydroxyapatite, the stoichiometric one, (which generally crystallizes in the hexagonal system) the value of Ca/P molar ratio is 1.67 [8].

Recent studies have shown that the crystalline lattice of hydroxyapatite has an affinity for substitution of Ca^{2+} ions with various cations/anions such as Zn^{2+} , Ag^+ , Sm^{3+} , Mg^{2+} , Eu^{3+} , F^- , Cl^- , etc. [8–14]. In practice, this substitutions are usually used to enhance the properties of hydroxyapatite [10,15,16]. Among the particularities of the HAp structure we mention the nanometric crystalline domain size, high surface reactivity, purity, solubility, etc. [9,10]. In addition to these properties, the biological ones are added, such as: biocompatibility, biodegradability, osteoconductivity, osteoinductivity, non-allergenic, etc. [1–16].

Over time, the deposition of hydroxyapatite by different methods including, sol-gel method, plasma spraying, thermal evaporation or performing magnetron sputtering techniques [16–24]. As the biocompatible, antibacterial or mechanical properties of hydroxyapatite need to be improved, these techniques are in continuous developing.

Radio frequency (rf) magnetron sputtering technique is a low deposition rate method, widely used for the generation of HAp or Hap-based coatings on substrates with different shapes and types [16–19]. Usually, the layers are compact with no cracks, pure and with good adhesion to the substrate [16–19]. By using more than one sputtering targets simultaneously, in the same deposition process, the incorporation of antimicrobial ions into the HAp structure have been performed [20,21]. Moreover, studies reported in the literature have highlighted that obtaining new coatings of hydroxyapatite, that are doped with various antimicrobial agents, with superior properties and potential applications in the medical field [20,22,23].

The results of different studies, presented in literature, have demonstrated that in the group of rare earths (lanthanides), there are elements with bear unique physical properties (magnetic, optical, catalytic, etc.) that allow lanthanides to be used in biomedical field (e.g., therapy, imaging and diagnosis, in drug/gene delivery systems, etc.) [23,24]. Samarium (Sm^{3+}) is an abundant chemical element with similar ionic radii to Ca^{2+} and radioactive properties, and with affinity for bone tissue [24]. Also, due to the f-f orbital transitions, lanthanides elements possess unique luminescent properties, which makes them suitable for application in bioimaging [25,26].

Due to their valuable properties, the complex materials that have in their composition samarium have been proposed for the treatment of various neoplasms (lung, prostate, breast, osteosarcoma, etc.) [24,27]. Also samarium complexes were used in pain therapy in cancers with bone metastases [24]. Moreover, previous studies have reported that the presence of Sm^{3+} ions in the structure of hydroxyapatite led to improved antimicrobial activity of HAp against bacterial strain [28], such as *Escherichia coli*, *Staphylococcus aureus*, *Bacillus cereus*, *Staphylococcus epidermidis*, *Salmonella typhi*, etc. [27–30]. The last studies [11,27,29–33] revealed that the antimicrobial activity of bioceramics, based on Sm-doped hydroxyapatite, depends on several factors, an important role being played by the antimicrobial agent which in our case is Sm. Moreover, the best results are obtained in samples with high concentrations of Sm^{3+} [7,10–12,27,29–33]. In this research, the physico-chemical and antibacterial properties of Sm-HAp layers generated by rf magnetron sputtering discharges are analyzed and presented. The sputtering target was a Sm-Hap tablet with $x_{\text{Sm}} = 0.05$ (5Sm-HAp). Previously, we reported Sm doped hydroxyapatite layers, with antifungal properties, obtained by thermal evaporation [7] or spin coating technique [21].

Studies showing that the 5Sm-HAp coatings obtained by magnetron sputtering technique retain the antimicrobial properties of the 5Sm-HAp suspension are presented for the first time in this study. Moreover, suspensions, target and coatings of 5Sm-HAp were examined by various techniques. The stability of the suspensions was assessed by ultrasound measurements. Information on the surface topography and sample composition was obtained by scanning electron microscopy (SEM). Elemental

composition of the coating were evaluated by Glow Discharge Optical Emission Spectroscopy (GDOES) and X-ray photoelectron spectroscopy (XPS). The vibrational modes are usually detected using Fourier transform infrared (FTIR) spectroscopy. On the other hand, the study of the antibacterial properties of suspensions, target and coatings based samarium doped hydroxyapatite against different microbial strains such as Gram negative bacterial strain *Escherichia coli* ATCC 25922, Gram positive bacterial strain *Staphylococcus aureus* ATCC 25923 and fungal strain *Candida albicans* ATCC 10,231 led to the conclusion that these materials are promising by their proven antimicrobial properties.

2. Materials and Methods

2.1. Materials

Ammonium hydrogen phosphate, $(\text{NH}_4)_2\text{HPO}_4$ (Sigma Aldrich, St. Louis, MO, USA, $\geq 99.0\%$), calcium nitrate tetrahydrate, $\text{Ca}(\text{NO}_3)_2 \cdot 4\text{H}_2\text{O}$ (Sigma Aldrich, St. Louis, MO, USA, $\geq 99.0\%$), samarium nitrate hexahydrate, $\text{Sm}(\text{NO}_3)_3 \cdot 6\text{H}_2\text{O}$ (Alpha Aesar, Germany, 99.97% purity), ammonium hydroxide, NH_4OH [Sigma Aldrich, St. Louis, MO, USA, 25% NH_3 in H_2O (T)], ethanol absolute, and double distilled water were used as precursors in the obtaining of $\text{Ca}_{10-x}\text{Sm}_x(\text{PO}_4)_6(\text{OH})_2$.

2.2. Samarium Doped Hydroxyapatite (Sm-HAp)

The synthesis process of samarium doped hydroxyapatite (5Sm-HAp) nanoparticles, $\text{Ca}_{10-x}\text{Sm}_x(\text{PO}_4)_6(\text{OH})_2$ with $x_{\text{Sm}} = 0.05$, was performed using an adapted method [9]. The $(\text{Ca} + \text{Sm})/\text{P}$ molar ratio was set to 1.67 [30,34,35]. The pH value of the resulting solution by adding the $\text{Ca}(\text{NO}_3)_2 \cdot 4\text{H}_2\text{O}$ and $\text{Sm}(\text{NO}_3)_3 \cdot 6\text{H}_2\text{O}$ dissolved in ethanol absolute into a solution of $(\text{NH}_4)_2\text{HPO}_4$, was kept constant at 11 by adding NH_4OH . The resulting solution was stirred, centrifuged and redispersed in deionized water. The stability and morphology of final resulting solution after stirred at 100°C for 24 h were analyzed. In order to obtain the coatings by magnetron sputtering technique, the target was prepared from the powders resulting from final resulting solution.

2.3. Thin Layer of 5Sm-HAp

By magnetron sputtering technique were generated 5Sm-HAp thin films on Si substrates. It was used a 2 inches magnetron source (acquired from K.J. Lesker Company, East Sussex, UK) coupled to a RF power supply at 50 W power. The 5Sm-HAp powder was pressed in air for few minutes and treated at 500°C in air in order to obtain the target. The depositions in rf magnetron sputtering discharge were performed in Ar gas flow (6 mln/min) and working pressure of 4×10^{-3} mbarr (base pressure $\sim 10^{-5}$ mbarr) in a 3 h single run. The distance between the magnetron source and grounded substrate holder was of 8 cm. The experimental set-up of the deposition chamber was presented in a previous study [22]. It was found that during the deposition process, the temperature at the substrate support increases. During the deposition process, the temperature at the substrate support was measured using a thermocouple. After one hour from the beginning of the deposition, the temperature at the substrate support was equal to 125°C . After three hours this temperature reached 135°C . Finally, the 5Sm-HAp coatings were treated for 4 h at 700°C .

2.4. Characterization Methods

Using a HITACHI S2600N-type microscope equipped with an energy dispersive X-ray attachment EDAX/2001 the morphology of the samples was evaluated and the elemental composition was determined of the samples. The morphology of the targets used to obtain the coatings and of the coatings was assessed by atomic force microscopy (AFM) studies using an NT-MDT NTEGRA Probe Nano Laboratory instrument (NT-MDT, Moscow, Russia). The measurements were conducted with the aid of a silicon NT-MDT NSG01 cantilever (NT-MDT, Moscow, Russia) in non-contact mode. The used silicon NT-MDT NSG01 cantilever is coated with a 35 nm gold layer. The data was acquired on a surface area of $15 \times 15 \mu\text{m}^2$ and the analysis were performed with Gwyddion 2.55 software

(Department of Nanometrology, Czech Metrology Institute, Brno, Czech Republic) [36]. All the studies were effectuated in air at 22 °C.

The 5Sm-HAp thin films molecular structure was examined in the 400–4000 cm^{-1} spectral range by FTIR-ATR spectroscopy using a Perkin Elmer SP-100 spectrometer (Perkin Elmer, Waltham, MA, USA). The processing of the obtained spectra was performed in accordance with the model presented in previous studies [16]. Using a GD Profiler in certain operation conditions such as: 650 Pa, 35 W RF power impulse mode at 1 kHz, and a duty cycle of 0.25 it was performed a depth profile analysis of 5Sm-HAp coatings.

The XPS surveys were achieved using SCIENCE SES 2002 system (Scienta Omicron, Taunusstein, Germany) and a monochromatic source of the X-ray radiation Al $K\alpha$ ($h\nu = 1486.6$ eV). All analyzed XPS spectra were calibrated according to the binding energies of C–C, C–H for carbon (C1s) that is equal to 284.8 eV. The analysis of the resulting data was performed using the Casa XPS 2.3.14 software (Shirley background type, Casa Software Ltd., Teignmouth, UK).

2.5. In Vitro Antimicrobial Activity

The antimicrobial properties of the samples were evaluated using the *Escherichia coli* ATCC 25922, *Staphylococcus aureus* ATCC 25923 and *Candida albicans* ATCC 10,231 microbial strains. An adapted diffusion method [37] was used in order to effectuate the qualitative assays. An adapted standard method [38] was used to perform quantitative assays [15]. The antimicrobial quantitative assays were evaluated by exposing the samples to 1.5 mL of 5×10^6 CFU/mL microbial suspension in Phosphate-buffer Saline (PBS). Subsequently, the microbial suspension was collected at various time intervals (12, 24 and 48 h) and incubated for 24 h on LB agar medium. A free microbial culture was used as positive control (C+). The number of colony forming units per milliliter (CFU/mL) was finally determined. All experiments were given in triplicate. The results were exhibited as mean \pm SD.

2.6. Statistical Analysis

All experiments were performed three times. Statistical analysis was performed using the *t*-test. A significant difference between samples was considered at $p < 0.05$. The *t*-test statistical analyses were performed using Office Excel 2013 software.

3. Results and Discussions

Figure 1 shows both the SEM image of the 5Sm-HAp particles in suspension, the surface of the target (which was obtained by pressing the obtained powder and the concentrated suspension) and the surface of the coating (obtained from the target by magnetron sputtering technique).

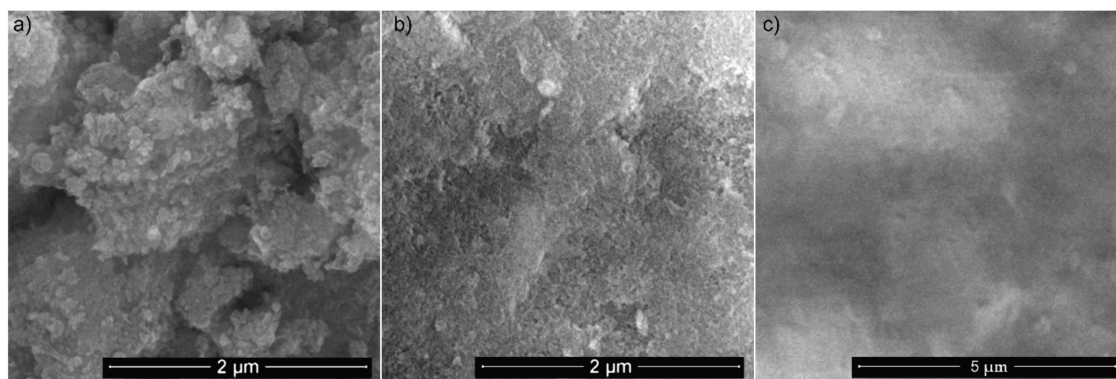


Figure 1. SEM micrographs of 5Sm-HAp as suspension (a) target (b) and coatings (c).

Conclusive evidence on the shape and uniformity of 5Sm-HAp particles was obtained following analysis of a drop of the suspension acquired from the synthesis process. The drop from the concentrated

suspension was deposited on a carbon band and dried under vacuum before being investigated. From SEM observation of 5Sm-HAp suspension (Figure 1a), the particles at nanometric scale with slightly ellipsoidal shape were identified. The SEM images (Figure 1b) of 5Sm-HAp target presented the uniform surface with nanoparticles that preserve the shape of the nanoparticles in suspension. Scanning electron micrographs exhibited in Figure 1c revealed that the 5Sm-HAp coating maintained the morphology of target as expected following the use of this coating technique.

The three-dimensional (3D) representation of the SEM surface topographies of 5Sm-HAp suspension, target and coatings presented in Figure 2a–c suggested that the suspension consists of nanometric particles presenting an ellipsoidal shape morphology (Figure 2a). It meant that the surface of the target is also homogenous with no visible imperfections and that the layers have the aspect of a uniform coating presenting no fissures, cracks or other visible imperfections.

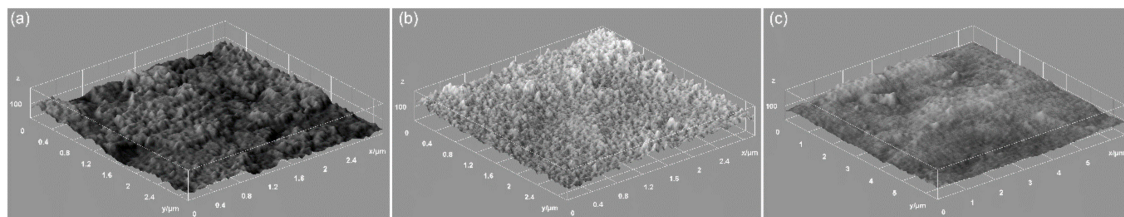


Figure 2. 3D representation of SEM micrographs of 5Sm-HAp as suspension (a) target (b) and coatings (c).

Energy dispersive X-ray spectroscopy (EDX) elemental mapping proved that the Sm, Ca, P and O on the surface of 5Sm-HAp coatings was distributed uniformly (Figure 3). The EDX elemental mapping analysis also highlighted that the Sm was uniformly doped onto the surface of the coatings. The complete picture of element maps for 5Sm-HAp coatings give clear information on the main constituent elements (O, Ca, P and Sm) of the 5Sm-HAp coating (Figure 3a–d). Furthermore, the EDX elemental mapping confirms the homogeneous distribution of the constituent elements at surface of 5Sm-HAp coatings.

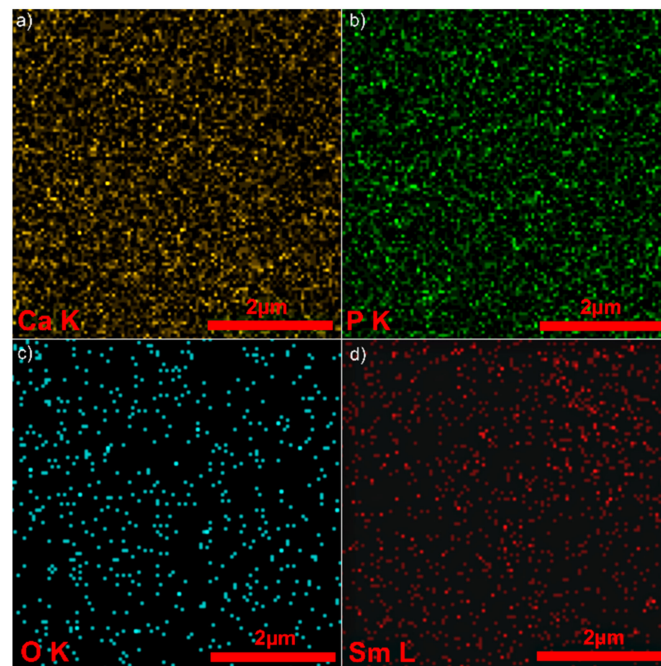


Figure 3. 2D elemental maps images of 5Sm-HAp coatings. (a) Ca; (b) P; (c) O; (d) Sm.

The 5Sm-HAp target and coatings were studied using AFM analysis. The two-dimensional (2D) and 3D AFM surface topography of the 5Sm-HAp target and layers are depicted Figure 4a,b. Moreover,

using the Gwydion software [36], a 3D representation of the 2D surface topography of both 5Sm-HAp target and coatings were realized and shown in Figure 4c,d. The 2D images of the surface morphology of 5Sm-HAp coatings, as well as the 3D representation highlighted that the 5Sm-HAp coatings have presented a surface morphology of a uniform coatings, without cracks, fissures or other defects. Besides, the 2D and 3D images of the surface morphology, obtained by AFM analysis of the target used for the coatings deposition, highlighted that the target had a uniform surface morphology without discontinuities. The AFM topography of registered on a surface of $15 \times 15 \mu\text{m}^2$ of 5Sm-HAp coatings (Figure 4b) emphasized that the surveyed area of the coating's surface did not present any irregularities or fissures thus suggesting the obtaining of a uniform and homogenous surface of nanometric size.

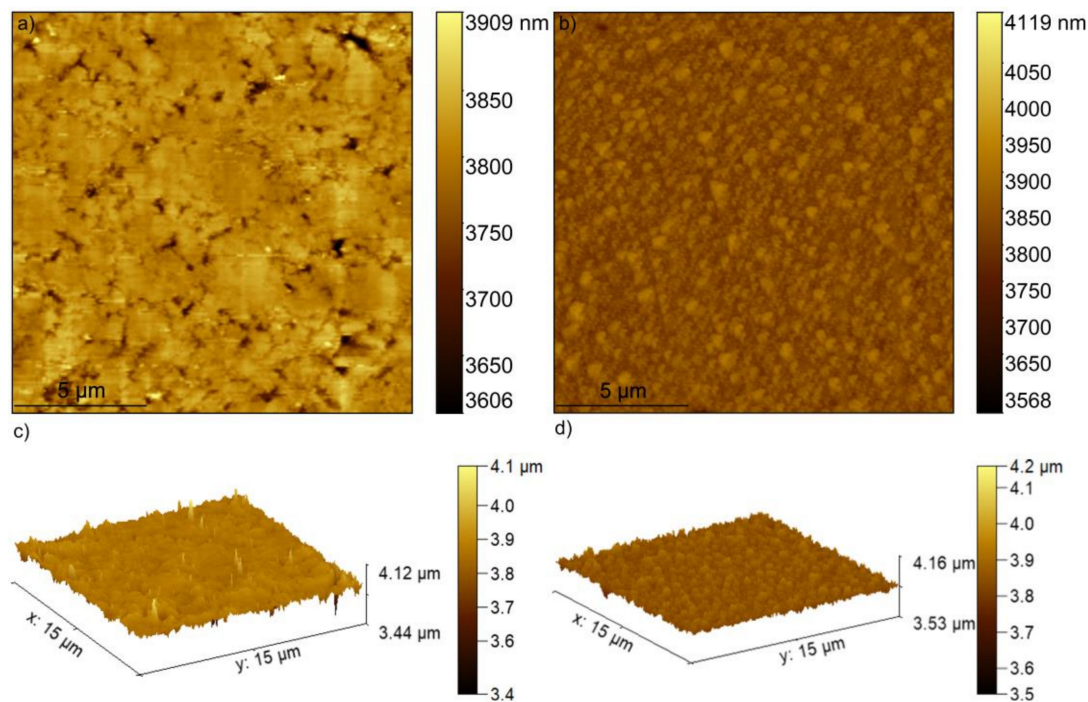


Figure 4. Topographical images of 5Sm-HAp target (a) and coatings (b) obtained by AFM and 3D representation of the topographical images of 5Sm-HAp target (c) and coatings (d).

The study of hydroxyapatite compounds by FTIR spectroscopy involve mainly investigations in the spectral range between $450\text{--}1200 \text{ cm}^{-1}$, due to P–O bond vibrations in the $[\text{PO}_4]^{3-}$ groups. The corresponding vibrational modes are usually detected at: 470 cm^{-1} (ν_2), $500\text{--}630 \text{ cm}^{-1}$ (ν_4), 960 cm^{-1} (ν_1), $1000\text{--}1100 \text{ cm}^{-1}$ (ν_3) [39,40]. The $[\text{CO}_3]^{2-}$ and OH^- groups also encountered into the HAp structure manifest IR vibrational bands at 1400 and 1630 cm^{-1} . The exact position of these IR bands that depend sometimes on the material type (bulk, powder or film), chemical and physical properties or doping concentration of the hydroxyapatite [4,14,18,37,41,42], can be revealed by curve fitting analysis. Such a theoretical assay is significant for uncover of the molecular structure of the investigated material.

The absorption IR spectrum of 5Sm-HAp sputtering target (Figure 5a) and 5Sm-HAp films obtained on Si substrates in magnetron sputtering discharge and the theoretical de-convoluted curves were shown (Figure 5b). The IR bands from 470 cm^{-1} (O–P–O bonding mode) and 1023 , 1090 cm^{-1} (P–O asymmetric stretching) observed into the absorption spectrum of 5Sm-HAp target (Figure 5a) are shifted to 474 respectively 1035 and 1101 cm^{-1} (Figure 5b) in the spectrum of 5Sm-HAp film. The molecular absorption band specific to P–O symmetric stretching vibrations from 960 cm^{-1} appear in both IR spectra of the 5Sm-HAp target precursor and film (Figure 5a,b). These IR bands was assigned to the vibrations in $[\text{PO}_4]^{3-}$ groups of the apatitic structure [42,43]. By multipeak fitting analysis of the 5Sm-HAp film spectrum it was found out other IR vibrational bands of P–O bonds

at 564 and 603 cm^{-1} specific to the apatitic structure and which belong to P–O internal vibrations. Figure 5b clearly illustrates the ν_4 mode (T2 symmetry) which is associated to the triple degenerate asymmetric O–P–O bending. The O–P–O bending vibrations manifest an absorption band at 560 cm^{-1} in the spectrum of 5Sm-HAp target (Figure 5a). The 1067 and 1101 cm^{-1} deconvoluted IR bands are characteristic to symmetric and asymmetric stretching vibrations of P–O in $[\text{PO}_4]^{3-}$. The P–O bond vibrations in non-apatitic phosphate structure [42] are identified by IR absorption bands from 1008 and 1118 cm^{-1} . The IR band from 735 cm^{-1} is attributed to $\text{P}_2\text{O}_7^{4-}$ group. Its presence in the IR spectra of HAp based layers was previously explained by the conversion of HPO_4^{2-} group in the plasma during the deposition process [42]. The IR from ~ 490 cm^{-1} could indicate the formation of Sm_2O_3 or SmPO_4 into the coating. In [44,45] were identified IR bands at 463 cm^{-1} (attributed to Sm_2O_3 formation) and 488 cm^{-1} (attributed to P(Sm)–O vibrations in SmPO_4).

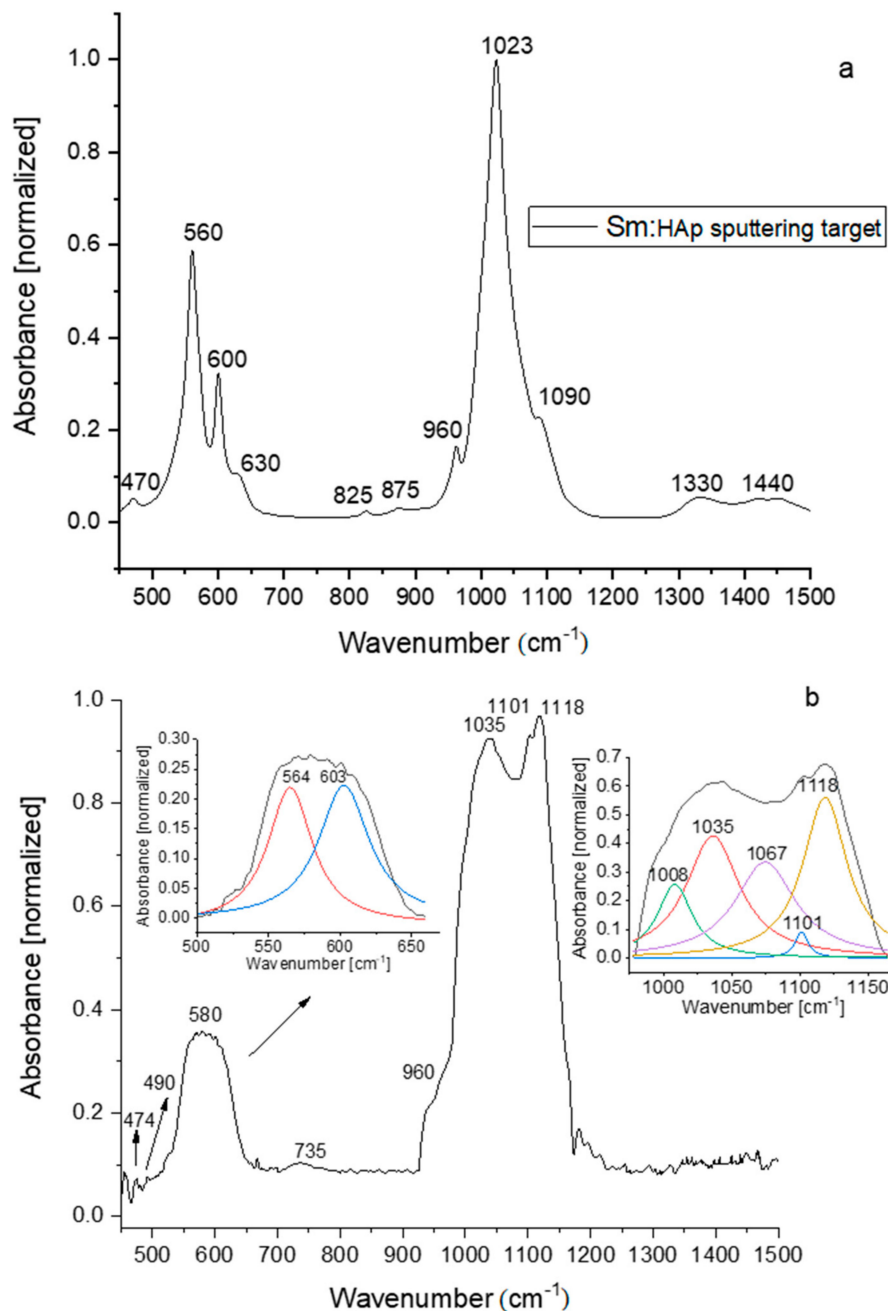


Figure 5. FTIR spectra of the 5Sm-HAp target material (a) and coatings (b).

Characterization of the 5Sm-HAp coatings in terms of distribution of chemical elements contained in the layer bulk was accomplished by GDOES. The depth profile curves of Ca, P, O, H, Ce and Si elements exhibit their presence from surface to substrate interface as function of sputtering time (Figure 6). The sample analysis area is usually of 4 mm in diameter. The interface zone between the 5Sm-HAp layer and the substrate is marked by the sharp increase of the Si depth profile. Until that point, the Ca, P, O and Ce depth profiles have similar compoment (see Figure 6). Some humps of Ca, P and Ce curves are observed at 5Sm-HAp/Si substrate interface simultaneous with the decreasing of C, O and H depth profile curves. It could indicate the diffusion/implantation of these elements into the Si substrate suggesting the formation of some interlinks between them.

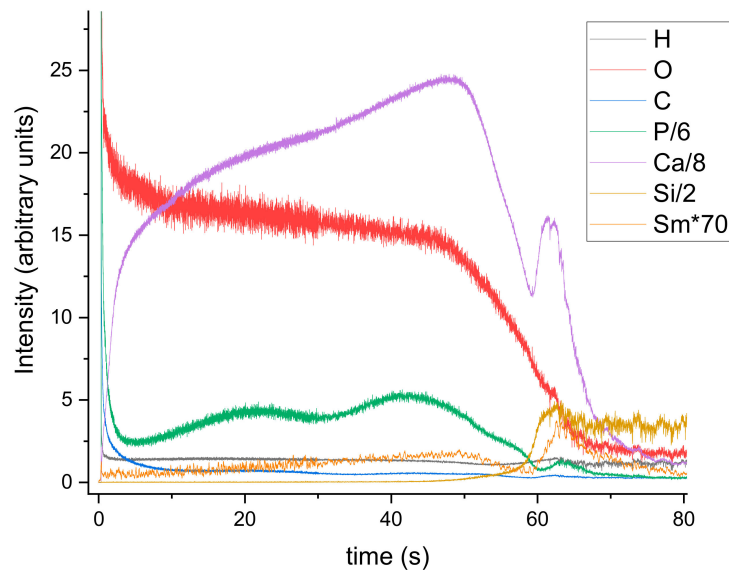


Figure 6. Depth profile of 5Sm-HAp coating on Si substrate achieved by radio frequency magnetron sputter.

XPS analysis was effectuate, to evaluate the elemental composition and chemical states of pure 5Sm-HAp coatings before and after etching (Figure 7).

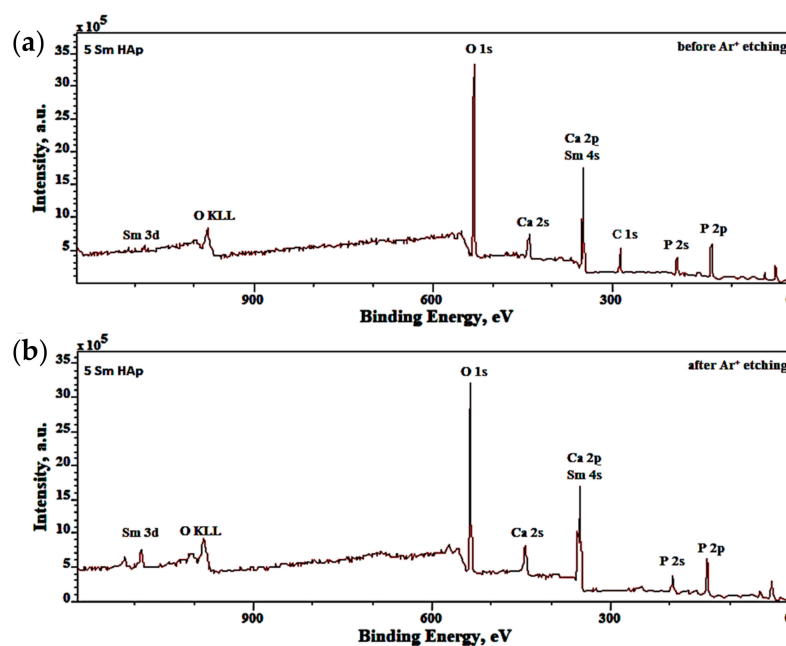


Figure 7. XPS survey spectra of 5Sm-HAp coating acquired before (a) and after (b) etching.

The XPS spectra of 5Sm-HAp coating before etching for P1s, P2p, Ca 2p, Sm 3d, O1s, were exhibited in Figure 7. As shown in Figure 8a the binding energies (BE) of P located at 134 eV and 190.7 eV were assigned to P 2p and P 2s. From Figure 8b the Ca XPS spectra of 5Sm-HAp coatings shows of two peaks at 147.3 eV and 350.7 eV that correspond to Ca 2p. In Figure 8c the Ce 3d consists of three symmetrical peaks located at BE of 1071.1 eV, 1083.1 eV and 1109.8 eV. The O1s XPS spectra of 5Sm-HAp coatings are showed in Figure 8d presents a peak was located at 530.8 eV.

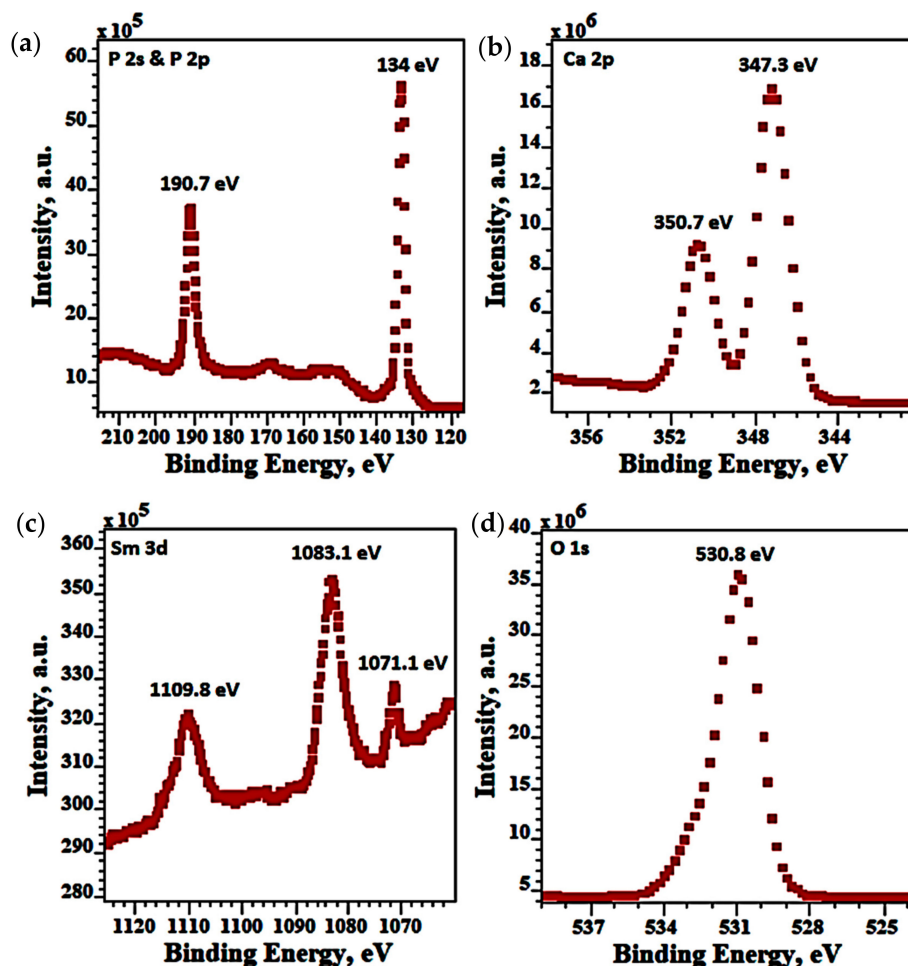


Figure 8. XPS spectra of 5Sm-HAp coatings before etching for P1s & P2p (a), Ca 2p (b), Sm 3d (c), O1s (d).

In Figure 8 the XPS spectra for P1s, P2p, Ca 2p, Sm 3d, O1s of 5Sm-HAp coatings after etching was showed. The BEs (binding energies) at 134.4 eV and 191.4 eV were assigned to P2p and P2s as can see in P XPS spectra of 5Sm-HAp coatings after etching (Figure 9a). The Ca XPS spectra of 5Sm-HAp coatings after etching correspond to Ca 2p and appears of two peaks at 147.3 eV and 350.7 eV (Figure 9b). The Sm 3d XPS spectra of 5Sm-HAp coatings after etching consists of two peaks at EB of 1083.9 eV and 1110.9 eV (Figure 9c). The BE of 532.0 corresponding O1s from O XPS spectra of 5Sm-HAp coatings after etching (Figure 9d).

The Ca 2p peaks related to Ca 2p_{3/2} (347.2–347.3 eV) and Ca 2p_{1/2} (350.7–351.3 eV) combined with the phosphorus and oxygen ones, i.e., P 2s (190.7–191.7 eV) and P 2p (133.1–134.7 eV) and O1s (530.8–532.1 eV), respectively, indicate the presence of Ca²⁺ ions, which most likely are in the Ca₁₀(PO₄)₆(OH)₂, and/or Ca₃(PO₄)₂, and/or Ca(H₂PO₄)₂ compounds (<https://srdata.nist.gov/xps>) as presented in previous studies (Table 1). In the Sm 3d spectrum, two distinct peaks are observed around Sm 3d_{5/2} (1082.9–1083.2 eV) and Sm 3d_{3/2} (1109.8–1110.1 eV) what can be interpreted as Sm³⁺, what may be indicated as calcium-phosphate structures enriched with Sm³⁺ ions. The peak recorded on

non-etched surface for binding energy equal to 1071.1 eV, most likely is dedicated to sodium compounds (NaH_2PO_2 , Na_2HPO_4), which should be treated as contamination (<https://srdata.nist.gov/xps>).

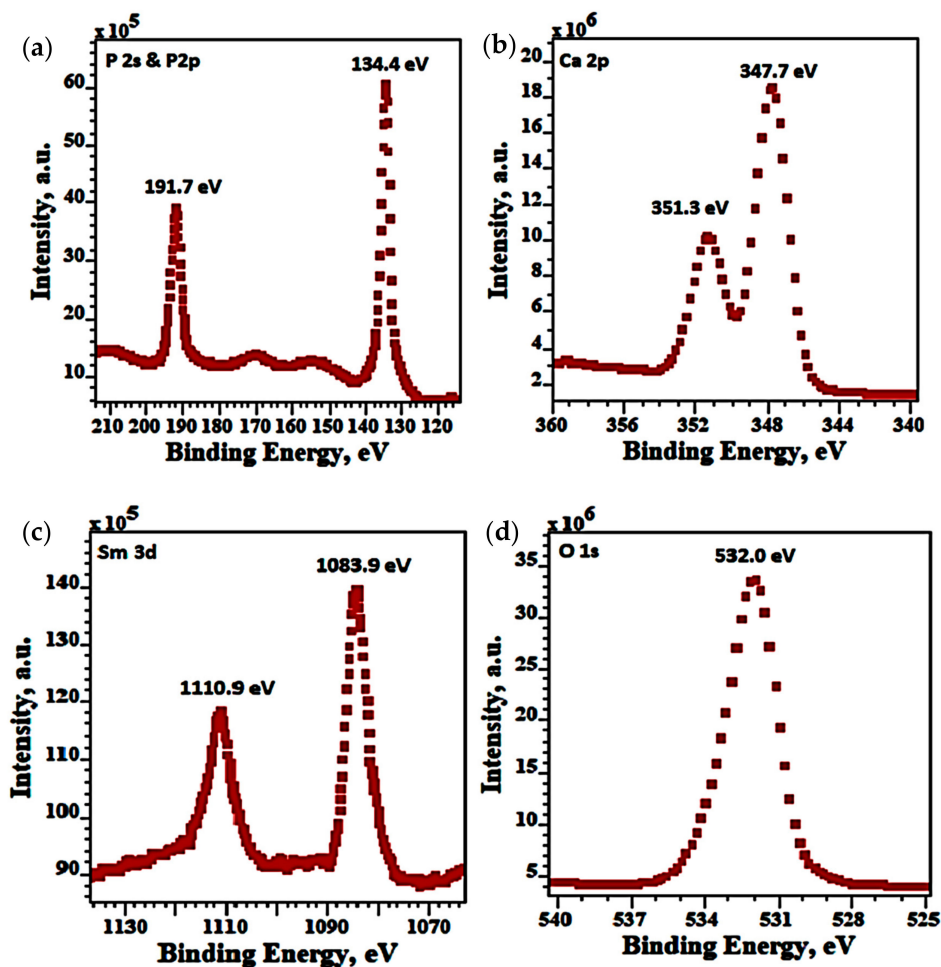


Figure 9. XPS spectra of 5Sm-HAp coatings after etching for P1s & P2p (a), Ca 2p (b), Sm 3d (c), O1s (d).

Table 1. Existing bioceramic compounds Ca-P [45–50].

Chemical Formula	Ca/P
$\text{Ca}(\text{H}_2\text{PO}_4)_2 \cdot \text{H}_2\text{O}$	0.5
$\text{Ca}(\text{H}_2\text{PO}_4)_2$	0.5
$\text{Ca}(\text{H}_2\text{PO}_4)_2$	0.5
$\text{CaHPO}_4 \cdot 2\text{H}_2\text{O}$	1.0
$\text{Ca}_8\text{H}_2(\text{PO}_4)_6 \cdot 5\text{H}_2\text{O}$	1.3
$\alpha\text{-Ca}_3(\text{PO}_4)_2$, $\beta\text{-Ca}_3(\text{PO}_4)_2$	1.5
$\text{Ca}_9(\text{PO}_4)_6$	1.5
$\text{Ca}_{10-x}(\text{HPO}_4)_x(\text{PO}_4)_{6-x}(\text{OH})_{2-x}$ ($0 < x < 1$)	1.5–1.67
$\text{Ca}_{10}(\text{PO}_4)_6(\text{OH})_2$	1.67
$\text{Ca}_{10}(\text{PO}_4)_6\text{F}_2$	1.67
$\text{Ca}_{10}(\text{PO}_4)_6\text{O}$	1.67
$\text{Ca}_4\text{O}(\text{PO}_4)_2$	2.0
$\text{Ca}_x\text{H}_y(\text{PO}_4)_z \cdot n\text{H}_2\text{O}$, $n = 3\text{--}4.5$; 15–20% H_2O	1.0–2.2

Quantitative analysis (Table 2) clearly indicates that the obtained calcium-phosphate structures are enriched with samarium (Sm^{3+}), which in atomic percentage content, varies in the top layer from 0.2 up

to 0.4 at%, while in the deeper layers from 0.7 to 1.1 at%. The data presented in Table 2 were obtained after performing 82 measurements for the samarium, calcium and phosphorus spectra, what was taken in to statistical analysis by the XPS equipment. The information in Table 1 indicates that the ratio $(Ca + Sm)/P$ is within 1.2–1.33, and the possibility of existence of the above described calcium phosphate-like structures, enriched in samarium. Considering that the Ca/P ratio provides information on the bioceramic compound, the XPS results show that the obtained layers do not keep the structure of pure hydroxyapatites, $Ca_{10}(PO_4)_6(OH)_2$, (Ca/P = 1.67). In our study, the XPS results showed that the bioceramic layer obtained has a deficient structure in Ca (Ca/P = 1.33) of the type $Ca_8H_2(PO_4)_6 \cdot 5H_2O$ known as hydroxyapatite is the most stable calcium phosphate [51,52]. Since HAp is the most stable form of calcium phosphate, found in human bones, we can say that the bioceramic coating obtained is a Ca-deficient hydroxyapatite that retains its biological properties.

Table 2. Quantitative analysis of XPS data.

Elements	5 Sm-HAp	
	Before Ar+ Etching	After Ar+ Etching
P	18.3	18.1
Ca	21.8	23.1
Sm	0.2	0.7
O	59.7	58.1

In recent years, due to the emergence of multidrug resistant microorganisms, significant concern worldwide has been drawn towards the development of novel and efficient antimicrobial agents. Studies conducted, to date, have deemed great candidates for use as antimicrobial agents of various types of composites materials, having ions in their composition, which exhibit antimicrobial activity. Nonetheless, studies are still scarce and there is still need to investigate further, in order to accomplish the development of a successful antimicrobial agent that could be used without posing any treat to living organisms or surrounding environments. The present research focuses on the preparation of novel samarium doped based hydroxyapatite coatings for biomedical applications. For this purpose, the antimicrobial properties of the 5Sm-HAp suspensions, targets and coatings were evaluated by being tested against reference microbial strains *Escherichia coli* ATCC 25922, *Staphylococcus aureus* ATCC 25923 and *Candida albicans* ATCC 10231. The qualitative antimicrobial assays studies of the 5Sm-HAp suspensions, targets and coatings are presented in Figures 10–12. The results of the antimicrobial studies revealed that all the samples presented good inhibitory activity on the tested strains.

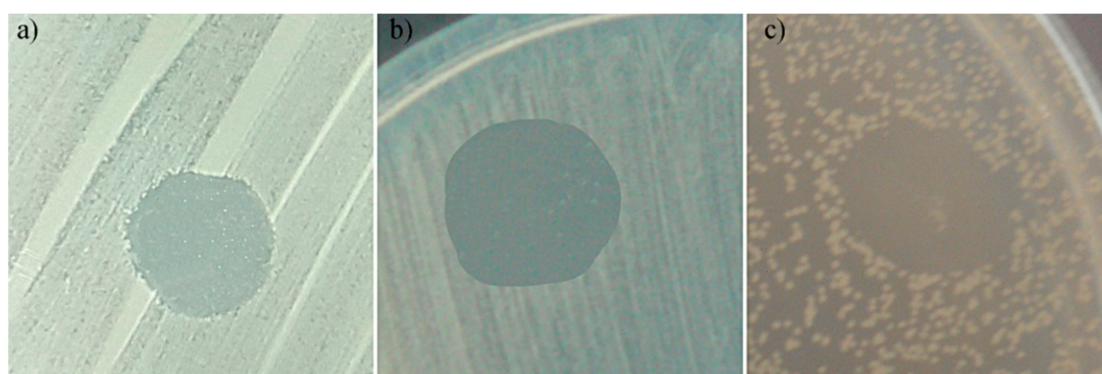


Figure 10. Antimicrobial activity of 5Sm-HAp suspensions against *Escherichia coli* ATCC 25922; (a) *Staphylococcus aureus* ATCC 25923; and (b) *Candida albicans* ATCC 10231 (c).

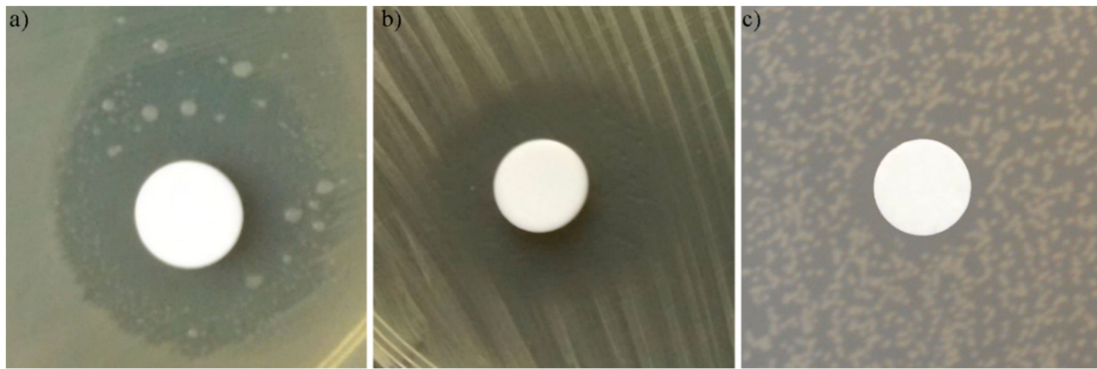


Figure 11. Antimicrobial activity of 5Sm-HAp target against *Escherichia coli* ATCC 25922; (a) *Staphylococcus aureus* ATCC 25923; and (b) *Candida albicans* ATCC 10231 (c).

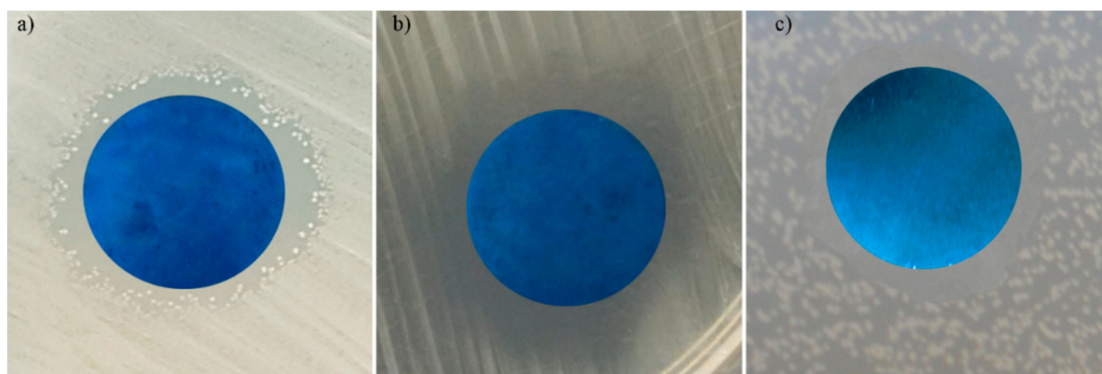


Figure 12. Antimicrobial activity of 5Sm-HAp coatings against *Escherichia coli* ATCC 25922; (a) *Staphylococcus aureus* ATCC 25923; and (b) *Candida albicans* ATCC 10231 (c).

The data of the qualitative assays revealed that, after 48 h of incubation the 5Sm-HAp suspensions, targets and coatings presented significant inhibition zone for all microbial strains that were tested. Furthermore, the data suggested that the diameters of the inhibition zones had better sizes in the case the Gram negative *Escherichia coli* ATCC 25922 and Gram positive *Staphylococcus aureus* ATCC 25923 bacterial strains than in the fungal strain *Candida albicans* ATCC 10231. The diameters obtained for the inhibition zones were clearly bigger in the case of *Escherichia coli* ATCC 25922 and *Staphylococcus aureus* ATCC 25923 bacterial strains, compared to ones obtained for the *Candida albicans* ATCC 10231 (Figure 10a–c, Figures 11a–c and 12a–c).

The data of the qualitative assays showed that the diameter of the inhibition zones obtained in the case of 5Sm-HAp suspensions were around 21 ± 2 mm in the case of *Escherichia coli* ATCC 25922, 25 ± 1.7 mm in the case of *Staphylococcus aureus* ATCC 25923 strains and 20.5 ± 1.5 mm for *Candida albicans* ATCC 10231.

A similar behavior was observed in the case of pressed pellet where, the obtained inhibition diameter of 21.2 ± 1.5 mm for *Escherichia coli* ATCC 25922, 17 ± 2.2 for *Staphylococcus aureus* ATCC 25923 and 12.4 ± 1.8 for *Candida albicans* ATCC 10231. Furthermore, the results of the qualitative antimicrobial assays demonstrated that the inhibition zone diameter were 14.25 ± 1.4 , 13.71 ± 1.8 and 11.48 ± 1 for *Escherichia coli* ATCC 25922, *Staphylococcus aureus* ATCC 25923 and *Candida albicans* ATCC 10231.

The antimicrobial activity of the 5Sm-HAp suspension, target and coatings against *Escherichia coli* ATCC 25922 *Staphylococcus aureus* ATCC 25923 and *Candida albicans* ATCC 10231 were also evaluated using a quantitative antimicrobial assay. The antimicrobial properties of the samples were examined at different time intervals, in order to determinate their effectiveness in time. The studies were conducted for 12 h, 24 h and 48 h and the antimicrobial properties of the samples were quantified by assessing the

inhibitory effects exhibited by the suspension, targets and coatings on the colony forming unit (CFU) values of the microbial strains compared to a free microbial strain used as control (C+). The results from three independent experiments are presented in Figure 13a–c as mean \pm SD.

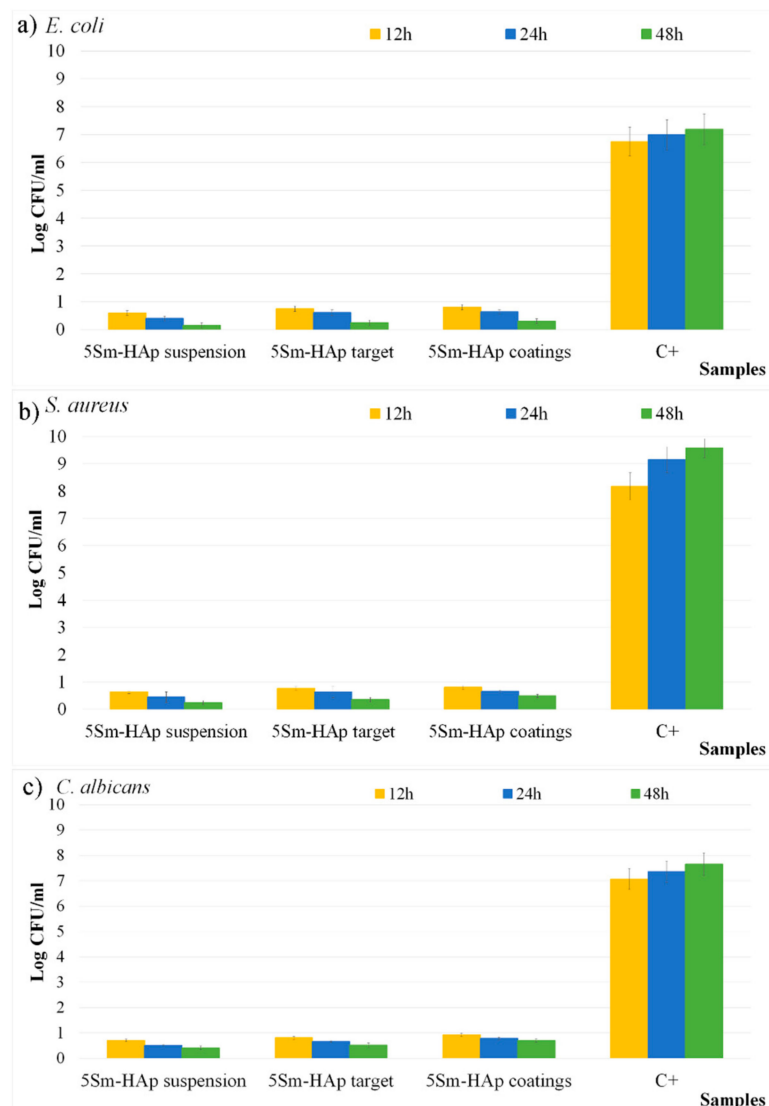


Figure 13. Antimicrobial activity of 5Sm-HAp suspension, target and coatings against *Escherichia coli* ATCC 25922; (a) *Staphylococcus aureus* ATCC 25923; (b) and *Candida albicans* ATCC 10231 (c) free microbial strain used as control (C+).

The results of the antimicrobial quantitative assays showed that the colony forming unity (CFU) proliferation was inhibited in the early phase of adherence (12 h) for all the tested samples regardless of their state (suspensions, target or coatings). Moreover, the data indicated that the 5Sm-HAp samples exhibited a noticeable antimicrobial activity and inhibited greatly the three microbial strains. These results led to the conclusion that the 5Sm-HAp tested samples have an inhibitory effect on the CFU development of Gram positive, Gram negative, as well as fungal strain making them perfect candidates for future research in the elaboration of novel antimicrobial agents. The colony forming unit count (CFUc) assay showed an important decrease in the number of colonies in the case of 5Sm-HAp suspension, target and coatings, compared to the number of colonies formed in the case of the free microbial culture (C+) used as control for all tested microorganisms. Furthermore, the results indicated that the inhibitory effect was dependent on the incubation time and the tested microbial strains. Therefore, the best inhibitory effect on the CFU development was obtained in the case

of *E. coli* bacterial strains followed by *S. aureus* and *C. albicans*. The results indicated that after 48 h the decrease of the Log CFU/mL had values smaller or close to 0.5 for all the samples and all the microbial strains.

These results are in good agreement with other similar studies regarding the potential antimicrobial activity of samarium ions or samarium based composites [27,29,53–58]. Moreover, the quantitative assays were in good agreement with the results obtained in the qualitative studies performed on 5Sm-HAp suspension, target and coatings. Moreover, the data suggested that the best antimicrobial activity was exhibited by the suspensions compared to the target and coatings. These could be due to the different interaction of the samples with the microbial cultures and also with the mechanisms responsible for the antimicrobial activity of the samples. Numerous studies have emphasized that both the physico-chemical properties of the samples such as state of aggregation, morphology, porosity, chemical structure, etc. have a great impact on the antimicrobial properties of materials [59–61].

Usually the antimicrobial active of nanoparticles have been attributed to their capacity to inhibit the wall/membrane of the microbial cells or to cause disruption of energy transduction, and also to their role in reducing the DNA production. In addition, the antimicrobial activity is usually associated with the ability of the materials to produce toxic reactive oxygen species (ROS). In our case the antimicrobial activity of the samples are attributed to the samarium ions presence in the HAp lattice. The results are confirmed due to the fact that in our previous reported on HAp solution, powders and coatings, no antimicrobial properties were visible for HAp samples [7,29,30]. The mechanism responsible for the antimicrobial properties of the 5Sm-HAp samples could be due to the action of the Sm^{3+} ions on the microbial cells wall/membrane (the cell integrity could be destroyed by direct contact between 5Sm-HAp nanoparticles and the microbial cell walls), ROS formation and also the release of antimicrobial ions, mainly Sm^{3+} , which could be responsible for DNA damage). Nonetheless, the existing studies regarding antimicrobial possible mechanisms are still scarce and there are reports with different results for various types of materials and coatings with various physico-chemical properties attributed to their morphology parameters. More than that, studies have also reported that there is a strong correlation on the antimicrobial properties and the synergy of the materials, coatings and substrate but this matter is still being disputed amongst researchers [62]. The results of our antimicrobial assays regarding the inhibitory effects of 5Sm-HAp suspensions, targets and coatings on Gram positive, Gram negative and fungal microbial strains have emphasized that all the tested samples presented good antimicrobial activity. Even though the antimicrobial activity of the 5Sm-HAp samples was attributed to the samarium ions presence in the HAp lattice, their intensity could be attributed to their other physico-chemical properties. Further, the results showed that the strongest antimicrobial activity was obtained for the suspensions compared to the targets and coatings on all the tested microbial strains. These results suggest that the 5Sm-HAp investigated samples are good candidates for creating antimicrobial agents with applications in the biomedical field both as suspensions, pressed pellets and coatings.

4. Conclusions

In order to conduct this research we used an adapted co-precipitation process to obtain 5Sm-HAp stable suspension. The target prepared from powder obtained from stable suspension were used to generate the 5Sm-HAp coatings on Si substrate via magnetron sputtering technique. The studies revealed that some Ca ions were substituted by Sm ions in hydroxyapatite crystal lattice successfully. The ultrasound measurements effectuated on the suspensions obtained following the synthesis method demonstrated the stability of 5Sm-HAp suspensions. The powders retains the ellipsoidal shape and nanometric size 5Sm-HAp nanoparticles in aqueous suspension. The 5Sm-HAp coatings exhibited a uniform surface. The XPS analysis of the coatings have shown that calcium-phosphate structures was enriched in Sm^{3+} ions. In agreement with SEM analysis the Sm ions was uniformly doped onto the surface of the coatings. Moreover the AFM examination of the surface morphology of the samples revealed that both the targets used to obtain the coatings and the coatings presented a homogenous

surface morphology. Furthermore, the antimicrobial assays emphasized that all the tested samples presented strong antimicrobial activity against *Escherichia coli* ATCC 25922, *Staphylococcus aureus* ATCC 25923 and *Candida albicans* ATCC 10231 microbial strains. More than that, the quantitative antimicrobial assays suggested that the best antimicrobial activity was observed for the 5Sm-HAp suspensions compared to the targets and coatings. Also, the data showed that all the samples exhibited strong inhibitory effect on the microbial CFU development starting with the first 12 h of incubation and that, the CFU development inhibition increased over time. The results of this study have shown that that the materials developed in this research could be used in medical applications, such as orthopedics and dentistry.

Author Contributions: Conceptualization, D.P., K.R., P.C., and S.G.; methodology, D.P., S.L.I., P.C., S.G., S.R., A.G., S.C.C., and K.R.; software, D.P., S.L.I., and A.G.; validation, D.P., P.C., S.G., S.R., S.L.I., A.G., S.C.C., and K.R.; formal analysis, D.P., S.L.I., S.G., S.R., A.G., and K.R.; investigation, D.P., P.C., S.G., S.R., S.L.I., A.G., S.C.C., and K.R.; resources, D.P., S.R., K.R., and P.C.; data curation, D.P., S.L.I., and A.G.; writing-original draft Preparation, D.P., S.L.I., A.G., S.R., and K.R.; writing-review and editing, D.P., P.C., S.G., S.L.I., K.R., and A.G.; Visualization, D.P., P.C., S.G., S.R., S.L.I., A.G., S.C.C., and K.R.; supervision, D.P., P.C., K.R., S.R., and A.G.; project administration, D.P., P.C., and K.R.; funding acquisition, D.P. All authors have read and agreed to the published version of the manuscript.

Funding: This research was partially funded by the Romanian Ministry of Research and Innovation with the grant number and project number PN-III-P1-1.2-PCCDI-2017-0629/contract no. 43PCCDI/2018.

Conflicts of Interest: The authors declare no conflict of interest.

References

1. Iconaru, S.L.; Prodan, A.M.; Turculet, C.S.; Beuran, M.R.; Ghita, V.; Costescu, A.; Groza, A.; Chifiriuc, M.C.; Chapon, P.; Gaiaschi, S.; et al. Enamel Based Composite Layers Deposited on Titanium Substrate with Antifungal Activity. *J. Spectrosc.* **2016**, *2016*, 4361051. [[CrossRef](#)]
2. Prodan, A.M.; Beuran, M.; Turculet, C.S.; Popa, M.; Andronesu, E.; Bleotu, C.; Raita, S.M.; Soare, M.; Lupescu, O. In Vitro Evaluation of Glycerol Coated Iron Oxide Nanoparticles in Solution. *Rom. Biotechnol. Lett.* **2018**, *23*, 13901–13908. [[CrossRef](#)]
3. Iconaru, S.L.; Turculet, C.; Le Coustumer, P.; Bleotu, C.; Chifiriuc, M.C.; Lazar, V.; Surugiu, A.; Badea, M.; Iordache, F.M.; Soare, M.; et al. Biological Studies On Dextrin Coated Iron Oxide Nanoparticles. *Rom. Rep. Phys.* **2016**, *68*, 1536–1544.
4. Raita, M.S.; Iconaru, S.L.; Groza, A.; Cimpeanu, C.; Predoi, G.; Ghegoiu, L.; Badea, M.L.; Chifiriuc, M.C.; Marutescu, L.; Trusca, R.; et al. Multifunctional Hydroxyapatite Coated with Artemisia absinthium Composites. *Molecules* **2020**, *25*, 413. [[CrossRef](#)]
5. Croitoru, A.-M.; Fikai, A.; Fikai, D.; Trusca, R.; Dolete, G.; Andronesu, E.; Turculet, S.C. Chitosan/Graphene Oxide Nanocomposite Membranes as Adsorbents with Applications in Water Purification. *Materials* **2020**, *13*, 1687. [[CrossRef](#)]
6. Stoleriu, S.; Lungu, C.; Ghitulica, C.D.; Surdu, A.; Voicu, G.; Cucuruz, A.; Turculet, C.S.; Ciocan, L.T. Influence of Dopant Nature on Biological Properties of ZnO Thin-Film Coatings on Ti Alloy Substrate. *Nanomaterials* **2020**, *10*, 129. [[CrossRef](#)]
7. Iconaru, S.L.; Stanciu, G.A.; Hristu, R.; Ghita, R.V. Properties of samarium doped hydroxyapatite thin films deposited by evaporation. *Rom. Rep. Phys.* **2017**, *69*, 508.
8. Tite, T.; Popa, A.-C.; Balescu, L.M.; Bogdan, I.M.; Pasuk, I.; Ferreira, J.M.F.; Stan, G.E. Cationic Substitutions in Hydroxyapatite: Current Status of the Derived Biofunctional Effects and Their in vitro Interrogation Methods. *Materials* **2018**, *11*, 2081. [[CrossRef](#)]
9. Predoi, D.; Iconaru, S.L.; Predoi, M.V.; Stan, G.E.; Buton, N. Synthesis, Characterization, and Antimicrobial Activity of Magnesium-Doped Hydroxyapatite Suspensions. *Nanomaterials* **2019**, *9*, 1295. [[CrossRef](#)]
10. Predoi, D.; Iconaru, S.L.; Predoi, M.V. Dextran-Coated Zinc-Doped Hydroxyapatite for Biomedical Applications. *Polymers* **2019**, *11*, 886. [[CrossRef](#)]
11. Turculet, C.S.; Prodan, A.M.; Negoii, I.; Teleanu, G.; Popa, M.; Andronesu, E.; Beuran, M.; Stanciu, G.A.; Hristu, R.; Badea, M.L.; et al. Preliminary Evaluation of The Antifungal Activity Of Samarium Doped Hydroxyapatite Thin Films. *Rom. Biotechnol. Lett.* **2018**, *23*, 13927–13932.

12. Prodan, A.M.; Iconaru, S.L.; Predoi, M.V.; Predoi, D.; Motelica-Heino, M.; Turculet, C.S.; Beuran, M. Silver-Doped Hydroxyapatite Thin Layers Obtained by Sol-Gel Spin Coating Procedure. *Coatings* **2020**, *10*, 14. [[CrossRef](#)]
13. Iconaru, S.L.; Groza, A.; Stan, G.E.; Predoi, D.; Gaiaschi, S.; Trusca, R.; Chifiriu, C.M.; Marutescu, L.; Tite, T.; Stanciu, G.A.; et al. Preparations of Silver/Montmorillonite Biocomposite Multilayers and Their Antifungal Activity. *Coatings* **2019**, *9*, 817. [[CrossRef](#)]
14. Iconaru, S.L.; Predoi, M.V.; Motelica-Heino, M.; Predoi, D.; Buton, N.; Megier, C.; Stan, G.E. Dextran-Thyme Magnesium-Doped Hydroxyapatite Composite Antimicrobial Coatings. *Coatings* **2020**, *10*, 57. [[CrossRef](#)]
15. Predoi, D.; Iconaru, S.L.; Predoi, M.V.; Buton, N.; Motelica-Heino, M. Zinc Doped Hydroxyapatite Thin Films Prepared by Sol-Gel Spin Coating Procedure. *Coatings* **2019**, *9*, 156. [[CrossRef](#)]
16. Surmenev, R.; Vladescu, A.; Surmeneva, M.; Ivanova, A.; Braic, M.; Grubova, I.; Cotrut, C.M. *Radio Frequency Magnetron Sputter Deposition as a Tool for Surface Modification of Medical Implants in Modern Technologies for Creating the Thin-film Systems and Coatings*; InTech: London, UK, 2017; pp. 1–36. [[CrossRef](#)]
17. Surmenev, R.A.; Surmeneva, M.A.; Grubova, I.Y.; Chernozem, R.V.; Krause, B.; Baumbach, T.; Epple, M. RF magnetron sputtering of a hydroxyapatite target: A comparison study on polytetrafluorethylene and titanium substrates. *Appl. Surf. Sci.* **2017**, *414*, 335–344. [[CrossRef](#)]
18. Groza, A.; Dreglici, D.B.; Ganciu, M. Calcium Phosphate Layers Deposited on Thermal Sensitive Polymer Substrates in Radio Frequency Magnetron Plasma Discharge. *Coatings* **2019**, *9*, 709. [[CrossRef](#)]
19. López, E.O.; Mello, A.; Sendão, H.; Costa, L.T.; Rossi, A.L.; Ospina, R.O.; Borghi, F.F.; Silva Filho, J.G.; Rossi, A.M. Growth of crystalline hydroxyapatite thin films at room temperature by tuning the energy of the RF-magnetron sputtering plasma. *ACS Appl. Mater. Interfaces* **2013**, *5*, 9435–9445. [[CrossRef](#)]
20. Robinson, L.; Salma-Ancane, K.; Stipniece, L.; Meenan, B.J.; Boyd, A.R. The deposition of strontium and zinc Co-substituted hydroxyapatite coatings. *J. Mater. Sci. Mater. Med.* **2017**, *28*, 51. [[CrossRef](#)]
21. Yuan, Q.; Qin, C.; Wu, J.; Xu, A.; Zhang, Z.; Liao, J.; Lin, S.; Ren, X.; Zhang, P. Synthesis and characterization of Cerium-doped hydroxyapatite/polylactic acid composite coatings on metal substrates. *Mater. Chem. Phys.* **2016**, *182*, 365–371. [[CrossRef](#)]
22. Gopi, D.; Sathishkumar, S.; Karthika, A.; Kavitha, L. Development of Ce³⁺/Eu³⁺ Dual-Substituted Hydroxyapatite Coating on Surgical Grade Stainless Steel for Improved Antimicrobial and Bioactive Properties. *Ind. Eng. Chem. Res.* **2014**, *53*, 20145–20153. [[CrossRef](#)]
23. Lu, Y.; Wang, E. Rare Earth Polyoxometalate Complexes. In *Rare Earth Coordination Chemistry: Fundamentals and Applications*; John Wiley & Sons: Singapore; Hoboken, NJ, USA, 2010; pp. 193–223. [[CrossRef](#)]
24. Wieszczycka, K.; Staszak, K.; Woźniak-Budych, M.J.; Jurga, S. Lanthanides and tissue engineering strategies for bone regeneration. *Coord. Chem. Rev.* **2019**, *388*, 248–267. [[CrossRef](#)]
25. Mondejar, S.P.; Kovtun, A.; Epple, M. Lanthanide doped calcium phosphate nanoparticles with high internal crystallinity and with a shell of DNA as fluorescent probes in cell experiments. *J. Mater. Chem.* **2007**, *17*, 4153–4159. [[CrossRef](#)]
26. Zantye, P.; Fernandes, F.; Roy Ramanan, S.; Kowshik, M. Rare Earth Doped Hydroxyapatite Nanoparticles for In Vitro Bioimaging Applications. *Curr. Phys. Chem.* **2019**, *9*, 94–109. [[CrossRef](#)]
27. Morais, D.S.; Coelho, J.; Ferraz, M.P.; Gomes, P.S.; Fernandes, M.H.; Hussain, N.S.; Santos, J.D.; Lopes, M.A. Samarium doped glass-reinforced hydroxyapatite with enhanced osteoblastic performance and antibacterial properties for bone tissue regeneration. *J. Mater. Chem. B* **2014**, *2*, 5872–5881. [[CrossRef](#)]
28. Predoi, D.; Iconaru, S.L.; Predoi, M.V. Bioceramic Layers with Antifungal Properties. *Coatings* **2018**, *8*, 276. [[CrossRef](#)]
29. Ciobanu, C.S.; Popa, C.L.; Predoi, D. Sm:HAp Nanopowders Present Antibacterial Activity against *Enterococcus faecalis*. *J. Nanomater.* **2014**, *2014*, 780686. [[CrossRef](#)]
30. Ciobanu, C.S.; Iconaru, S.L.; Popa, C.L.; Motelica-Heino, M.; Predoi, D. Evaluation of Samarium Doped Hydroxyapatite, Ceramics for Medical Application: Antimicrobial Activity. *J. Nanomater.* **2015**, *2015*, 849216. [[CrossRef](#)]
31. Balamurugan, A.; Sudha, M.; Surendhiran, S.; Anandarasu, R.; Ravikumar, S.; Syed Khadar, Y.A. Hydrothermal synthesis of samarium (Sm) doped cerium oxide (CeO₂) nanoparticles: Characterization and antibacterial activity. *Mater. Today Proc.* **2020**, *26*, 3588–3594. [[CrossRef](#)]
32. Predoi, D.; Iconaru, S.L.; Predoi, M.V.; Motelica-Heino, M. Removal and Oxidation of As(III) from Water Using Iron Oxide Coated CTAB as Adsorbent. *Polymers* **2020**, *12*, 1687. [[CrossRef](#)]

33. Iconaru, S.L.; Motelica-Heino, M.; Guegan, R.; Predoi, M.V.; Prodan, A.M.; Predoi, D. Removal of Zinc Ions Using Hydroxyapatite and Study of Ultrasound Behavior of Aqueous Media. *Materials* **2018**, *11*, 1350. [CrossRef] [PubMed]
34. Ciobanu, C.S.; Iconaru, S.L.; Massuyeau, F.; Constantin, L.V.; Costescu, A.; Predoi, D. Synthesis, structure, and luminescent properties of europium-doped hydroxyapatite nanocrystalline powders. *J. Nanomater.* **2012**, *2012*, 942801. [CrossRef]
35. Predoi, D.; Iconaru, S.L.; Predoi, M.V.; Motelica-Heino, M.; Guegan, R.; Buton, N. Evaluation of antibacterial activity of zinc-doped hydroxyapatite colloids and dispersion stability using ultrasounds. *Nanomaterials* **2019**, *9*, 515. [CrossRef] [PubMed]
36. Gwyddion. Available online: <http://gwyddion.net/> (accessed on 20 January 2020).
37. Predoi, D.; Popa, C.L.; Chapon, P.; Groza, A.; Iconaru, S.L. Evaluation of the Antimicrobial Activity of Different Antibiotics Enhanced with Silver-Doped Hydroxyapatite Thin Films. *Materials* **2016**, *9*, 778. [CrossRef]
38. ASTM International. *ASTM E2149–13a Standard Test Method for Determining the Antimicrobial Activity of Antimicrobial Agents under Dynamic Contact Conditions*; ASTM International: West Conshohocken, PA, USA, 2013.
39. Jastrzebski, W.; Sitarz, M.; Rokita, M.; Bułat, K. Infrared spectroscopy of different phosphates structures. *Spectrochim. Acta Part A* **2011**, *79*, 722–727. [CrossRef]
40. Berzina-Cimdina, L.; Borodajenko, N. Research of Calcium Phosphates Using Fourier Transform Infrared Spectroscopy. In *Infrared Spectroscopy—Materials Science, Engineering and Technology*; Theophile, T., Ed.; InTech: London, UK, 2012.
41. Monsees, T.K.; Ak Azem, F.; Cotrut, C.M.; Braic, M.; Abdulgader, R.; Pana, I.; Birlik, I.; Kiss, A.; Booyesen, R.; Vladescu, A. Biodegradable Ceramics Consisting of Hydroxyapatite for Orthopaedic Implants. *Coatings* **2017**, *7*, 184. [CrossRef]
42. Phatai, P.; Futralan, C.M.; Utara, S.; Khemthong, P.; Kamonwannasit, S. Structural characterization of cerium-doped hydroxyapatite nanoparticles synthesized by an ultrasonic-assisted sol-gel technique. *Results Phys.* **2018**, *10*, 956–963. [CrossRef]
43. Marzouk, M.A.; ElBatal, H.A.; Hamdy, Y.M.; Ezz-Eldin, F.M. Collective Optical, FTIR, and Photoluminescence Spectra of CeO₂ and/or Sm₂O₃-Doped Na₂O–ZnO–P₂O₅ Glasses. *Int. J. Opt.* **2019**. [CrossRef]
44. Babu, B.C.; Wang, G.-G.; Baker, A.P.; Wang, B.-L. Synthesis, photoluminescence, energy transfer and thermal stability of SmPO₄@SiO₂:Eu³⁺ core-shell structured red phosphors for WLEDs. *J. Alloys Compd.* **2018**, *766*, 74–87. [CrossRef]
45. Adelekea, S.A.; Bushroaa, A.R.; Sopyanb, I. Recent Development of Calcium Phosphate-Based Coatings on Titanium Alloy Implants. *Surf. Eng. Appl. Electrochem.* **2017**, *53*, 419–433. [CrossRef]
46. Kalita, S.J.; Bhardwaj, A.; Bhatt, H.A. Nanocrystalline Calcium Phosphate Ceramics in Biomedical Engineering. *Mater. Sci. Eng. C.* **2007**, *27*, 441–449. [CrossRef]
47. Dorozhkin, S.V. Calcium orthophosphates. *J. Mater. Sci.* **2007**, *42*, 1061–1095. [CrossRef]
48. Dorozhkin, S.V. Calcium orthophosphates in nature, biology and medicine. *Materials* **2009**, *2*, 399–498. [CrossRef]
49. Dorozhkin, S.V. Calcium Orthophosphates as Bioceramics: State of the Art. *J. Funct. Biomater.* **2010**, *1*, 22–107. [CrossRef]
50. Zhao, J.; Liu, Y.; Sun, W.B.; Zhang, H. Amorphous calcium phosphate and its application in dentistry. *Chem. Cent. J.* **2011**, *5*, 1–7. [CrossRef]
51. Ramselaar, M.M.A.; Driessens, F.C.M.; Kalk, W.; De Wijn, J.R.; Van Mullem, P.J. Biodegradation of four calcium phosphate ceramics; invivo rates and tissue interactions. *J. Mater. Sci. Mater. Med.* **1991**, *2*, 63–70. [CrossRef]
52. Rapacz-Kmita, A.; Paluszkiwicz, C.; Ślósarczyk, A.; Paszkiewicz, Z. FTIR and XRD investigations on the thermal stability of hydroxyapatite during hot pressing and pressureless sintering processes. *J. Mol. Struct.* **2005**, *744*, 653–656. [CrossRef]
53. Nakayama, M.; Smith, C.L.; Feltis, B.N.; Piva, T.J.; Tabatabaie, F.; Harty, P.D.; Gagliardi, F.M.; Platts, K.; Otto, S.; Blencowe, A.; et al. Samarium doped titanium dioxide nanoparticles as theranostic agents in radiation therapy. *Phys. Med.* **2020**, *75*, 69–76. [CrossRef]
54. Ciobanu, C.S.; Iconaru, S.L.; Predoi, D.; Prodan, A.M.; Predoi, M.V. Physico-Chemical Properties and In Vitro Antifungal Evaluation of Samarium Doped Hydroxyapatite Coatings. *Coatings* **2020**, *10*, 827. [CrossRef]
55. Kannan, S.; Nallaiyan, R. Anticancer Activity of Samarium-Coated Magnesium Implants for Immunocompromised Patients. *ACS Appl. Bio Mater.* **2020**, *3*, 4408–4416. [CrossRef]

56. Baranowska, A.; Kochanowicz, M.; Żmojda, J.; Miluski, P.; Wajda, A.; Leśniak, M.; Dorosz, D. Biological properties of rare-earth doped bioactive glass. In *Optical Fibers and Their Applications 2020*; International Society for Optics and Photonics: Tampa, FL, USA, 2020; Volume 11456, p. 1145604. [[CrossRef](#)]
57. Anand, V.; Sakthivelu, A.; Deva Arun Kumar, K.; Valanarasu, S.; Kathalingam, A.; Ganesh, V.; Shkir, M.; AlFaify, S.; Yahia, I.S. Rare earth Sm³⁺ co-doped AZO thin films for opto-electronic application prepared by spray pyrolysis. *Ceram. Int.* **2018**, *44*, 6730–6738. [[CrossRef](#)]
58. Sathishkumar, S.; Louis, K.; Shinyjoy, E.; Gopi, D. Tailoring the Sm/Gd-Substituted Hydroxyapatite Coating on Biomedical AISI 316L SS: Exploration of Corrosion Resistance, Protein Profiling, Osteocompatibility, and Osteogenic Differentiation for Orthopedic Implant Applications. *Ind. Eng. Chem. Res.* **2016**, *55*, 6331–6344. [[CrossRef](#)]
59. Donlan, R.M. Biofilms: Microbial life on surfaces. *Emerg. Infect. Dis.* **2002**, *8*, 881–890. [[CrossRef](#)] [[PubMed](#)]
60. Katsikogianni, M.; Missirlis, Y.F. Concise review of mechanisms of bacterial adhesion to biomaterials and of techniques used in estimating bacteria-material interactions. *Eur. Cells Mater.* **2004**, *8*, 37–57. [[CrossRef](#)]
61. Carlén, A.; Nikdel, K.; Wennerberg, A.; Holmberg, K.; Olsson, J. Surface characteristics and in vitro biofilm formation on glass ionomer and composite resin. *Biomaterials* **2001**, *22*, 481–487. [[CrossRef](#)]
62. Buergers, R.; Rosentritt, M.; Handel, G. Bacterial adhesion of *Streptococcus mutans* to provisional fixed prosthodontic material. *J. Prosthet. Dent.* **2007**, *98*, 461–469. [[CrossRef](#)]

Publisher's Note: MDPI stays neutral with regard to jurisdictional claims in published maps and institutional affiliations.



© 2020 by the authors. Licensee MDPI, Basel, Switzerland. This article is an open access article distributed under the terms and conditions of the Creative Commons Attribution (CC BY) license (<http://creativecommons.org/licenses/by/4.0/>).